Global parameter-space correlations of coherent searches for continuous gravitational waves.

Reinhard Prix and Yousuke Itoh

Max Planck Institut für Gravitationsphysik, Albert Einstein Institut,
Am Mühlenberg 1, Golm 14476, Germany

E-mail: Reinhard.Prix@aei.mpg.de

Abstract. The space of phase-parameters (sky-position, frequency, spindowns) of a coherent matched-filtering search for continuous gravitational waves from isolated neutron stars shows strong global correlations ("circles in the sky"). In the local limit this can be analysed in terms of a parameter-space metric, but the global properties are less well studied. In this work we report on our recent progress in understanding these global correlations analytically for short to intermediate (less than a month, say) observation times and neglecting spindowns. The *location* of these correlation-circles in parameter-space is found to be determined mostly by the orbital velocity of the earth, while the spin-motion of the detector and the antenna-patterns only contribute significantly to the amplitude of the detection statistic along these circles.

PACS numbers: 04.80.Nn, 95.75.-z
AEI publication number: AEI-2005-077

1. Introduction

Continuous gravitational waves from, for example, rotating neutron stars with non-axisymmetric deformations such as mountains or oscillation-modes, are one of the primary targets of current-generation detectors of both interferometric- (e.g. see [2, 3]) as well as bar-detector design [9].

In this paper we restrict ourselves to gravitational waves emitted from isolated neutron stars with negligible proper motion, for which the signal can be assumed to be a nearly monochromatic sinusoidal (with slowly decreasing frequency) in the solar-system barycenter frame (SSB). The corresponding signal received at the detector will be Doppler-modulated by the spin of the earth and its orbital motion around the sun. The phase of the received signal therefore depends not only on its intrinsic frequency f and spindowns $f^{(k)} \equiv d^k f/dt^k$, but also on the sky-position (denoted by α and δ for right ascension and declination) of the source and on the detector location. In addition there is a time-dependent amplitude modulation of the signal depending on its polarisation angle ψ and amplitudes h_+ and $h_\times$. However, as shown in [5], one can eliminate these "amplitude parameters" together with the initial phase of the signal Φ_0 by analytically maximising the detection statistic over these parameters. The resulting reduced parameter-space therefore only consists of the "phase parameters" $\mathcal{P} = \{\alpha, \delta, f, f^{(k)}\}$, and the corresponding partially maximised detection statistic is usually referred to as the "$\mathcal{F}$-statistic".

Given a stretch of data $x(t)$ from the detector, an untargeted search (as opposed to a search for known pulsars) consists of calculating the detection statistic $\mathcal{F}$ over the parameter space (by sampling individual points) and determining the location of "candidates" that cross a predetermined threshold. For a given signal $\mathcal{P}_\mathrm{s} = \{\alpha_\mathrm{s}, \delta_\mathrm{s}, f_\mathrm{s}, f_\mathrm{s}^{(k)}\}$, the detection statistic $\mathcal{F}$ in a search-point $\mathcal{P}$ generally depends on the parameter-mismatch $\Delta\mathcal{P} \equiv \mathcal{P}_\mathrm{s} - \mathcal{P}$, i.e., $\mathcal{F} = \mathcal{F}(\mathcal{P}_\mathrm{s}, \Delta\mathcal{P})$ (strictly speaking, $\mathcal{F}$ also depends on the amplitude parameters of the signal). Neglecting noise, one can expect $\mathcal{F}$ to be maximal for the perfectly matched search-point $\Delta\mathcal{P} = 0$. In the local neighbourhood of this point, the loss $\Delta\mathcal{F} \equiv \mathcal{F}(\mathcal{P}_\mathrm{s}, 0) - \mathcal{F}(\mathcal{P}_\mathrm{s}, \Delta\mathcal{P})$ in detection statistic can be quantified in terms of a parameter-space metric as discussed in [8, 4]. Namely, neglecting effects of the amplitude-parameters of the signal, this metric can be defined as $\Delta\mathcal{F}(\mathcal{P}_\mathrm{s}, \Delta\mathcal{P})/\mathcal{F}(\mathcal{P}_\mathrm{s}, 0) = \sum_{i,j} g_{ij}(\mathcal{P}_\mathrm{s})\, \Delta\mathcal{P}^i\, \Delta\mathcal{P}^j + \mathcal{O}(\Delta\mathcal{P}^3)$.

In the case of isolated neutron stars, we find that this metric is *highly* anisotropic in terms of the above parameter-space variables (in particular with respect to sky-position), as will also be seen in section 6. Furthermore, the global behaviour of $\mathcal{F}$ differs dramatically from the local quadratic decrease as a function of parameter-mismatch $\Delta\mathcal{P}$. This can be seen, for example, in figure 2 for an all-sky search at fixed frequency of an injected signal. For each target search-frequency f within the Doppler-window of the signal frequency f_s, one finds a very thin circular band on the sky along which $\mathcal{F}$ is of comparable magnitude to its maximum, while it drops sharply to zero in the directions orthogonal to this "circle". In the local limit this feature has already been pointed out in [7].

In this work we present an approximate analytic description of these "circles in the sky", tracing their physical origin to the Doppler-shift due to the orbital motion around the sun. The Doppler-shift induced by the spin-motion of the earth as well as the amplitude modulations due to the rotating antenna-pattern are found to give only very small corrections to the *structure* of these patterns in parameter-space (i.e., the location of the circles), while they do contribute significantly to the *amplitude* of the $\mathcal{F}$-statistic along these circles.

2. Matched filtering of continuous signals

The gravitational-wave strain $h(t)$ at the detector can be written in the form

$$h(t) = F_+(t)\, h_+(t) + F_\times(t)\, h_\times(t)\,, \tag{1}$$

where $F_{+,\times}$ are the antenna-pattern functions, and $h_{+,\times}$ are the two polarisation components of the gravitational wave. For a continuous pulsar-signal we can write

$$h_+(t) = A_+ \sin\left(\Phi(t) + \Phi_0\right)\,, \quad h_\times(t) = A_\times \cos\left(\Phi(t) + \Phi_0\right)\,. \tag{2}$$

The phase $\Phi(t)$ of the signal is assumed to be of the form

$$\Phi(t; f^{(k)}, \vec{n}) = 2\pi \sum_{k=0}^{s} \frac{f^{(k)}}{(k+1)!}\, \tau^{k+1}(t, \vec{n})\,, \tag{3}$$

where s is the number of spindown parameters, and τ is the arrival time in the solar-system barycenter (SSB) of a wave-front from direction $\vec{n} = (\cos\delta\cos\alpha, \cos\delta\sin\alpha, \sin\delta)$ arriving at the detector at time t, i.e.,

$$\tau(t, \vec{n}) \equiv t + \frac{\vec{r}(t)\cdot\vec{n}}{c}\,, \tag{4}$$

with $\vec{r}(t)$ denoting the vector from the SSB to the detector. As shown in [5], the full phase-model (3) can be simplified by an approximated model without significant loss in detection statistic, namely

$$\Phi(t) \approx 2\pi \left[\sum_{k=0} \frac{f^{(k)}}{(k+1)!} t^{k+1} + \frac{\vec{r}(t)\cdot\vec{n}}{c} \sum_{k=0} \frac{f^{(k)}}{k!} t^k \right] , \tag{5}$$

which will be dominated by the first term, i.e., $\Phi(t) \approx 2\pi f t$. In the case of stationary Gaussian noise, the likelihood ratio Λ (which is the optimal detection statistic in the sense of Neyman-Pearson) is given by

$$\ln \Lambda = \frac{T}{S_h} \left[(x||h) - \frac{1}{2}(h||h) \right] , \tag{6}$$

where S_h is the power spectral density of the noise, and the scalar product $(x||y)$ is defined as

$$(x||y) \equiv \frac{2}{T} \int_0^T x(t)\, y(t)\, dt \, . \tag{7}$$

3. Simplified matched-filtering statistic: neglecting amplitude modulations

In the following we make the simplifying assumption that we can neglect the amplitude-modulation caused by the antenna-pattern, so we assume $F_{+,\times} \approx$ const., and using (1) and (2) this results in the simplified strain model

$$h(t) = A_1 \cos\Phi(t) + A_2 \sin\Phi(t) \, . \tag{8}$$

Maximising the log-likelihood function (6) over the two unknown amplitudes $A_{1,2}$, we obtain

$$\ln \Lambda_{\mathrm{ML}} = \frac{T}{2S_h} \left| \left(x||e^{-i\Phi}\right) \right|^2 \equiv \frac{T}{2S_h} |X|^2 \, , \tag{9}$$

defining the matched-filtering amplitude X. In the following we assume the data contains only a unit-amplitude pulsar-signal of the form

$$x(t) = \Re[s(t)], \quad \text{with} \quad s(t) = \exp\left[i\, \Phi\left(t; f_{\mathrm{s}}^{(k)}, \vec{n}_{\mathrm{s}}\right) \right] , \tag{10}$$

characterised by the signal phase-parameters $f_{\mathrm{s}}^{(k)}$ and $\vec{n}_{\mathrm{s}}$. The matched-filtering amplitude X, defined in (9), can therefore be expressed as

$$X = \left(x||e^{-i\Phi}\right) \approx \frac{1}{T} \int s(t)\, e^{-i\Phi(t)}\, dt = \frac{1}{T} \int e^{i\Delta\Phi(t)}\, dt \, , \tag{11}$$

where $\Delta\Phi$ is the phase-difference $\Delta\Phi(t) = \Phi_{\mathrm{s}}(t) - \Phi(t)$, and where we have used the fact that $\int \exp[i2\pi(f+f_{\mathrm{s}})t]dt \approx 0$. We see from (11) that $|X|$ will have a global maximum of $|X| = 1$ if the phase-parameters of the template are perfectly matched to the signal, i.e., $\Delta\Phi = 0$, while $|X|$ will decrease very rapidly for increasing phase-mismatches.

The central aim of the following investigation is to determine the regions in parameter-space for which the detection statistic $|X|$ is of order unity for a given signal $\{\vec{n}_{\mathrm{s}},\, f_{\mathrm{s}}^{(k)}\}$.

4. Analytic approximation for $|X|^2$

In order to simplify the following discussion, we restrict ourselves in this study to pulsar-signals with negligible spindown over the observation period T, so we assume $f^{(k)} \approx 0$ for $k > 0$. Using (5), we can therefore write the phase-mismatch $\Delta\Phi(t)$ as

$$\Delta\Phi(t; \vec{n}_{\mathrm{s}}, f_{\mathrm{s}}; \vec{n}, f) = 2\pi \left[\Delta f \, t + \frac{\vec{r}(t)}{c} \cdot \vec{A} \right] , \tag{12}$$

where we defined

$$\Delta f \equiv f_{\mathrm{s}} - f \,, \quad \text{and} \quad \vec{A} \equiv f_{\mathrm{s}} \vec{n}_{\mathrm{s}} - f \vec{n} \,. \tag{13}$$

We can decompose the motion of the detector $\vec{r}(t)$ into its orbital- and spin-component, namely, $\vec{r}(t) = \vec{r}_{\mathrm{orb}}(t) + \vec{r}_{\mathrm{spin}}(t)$, where $\vec{r}_{\mathrm{orb}}$ is the vector from the SSB to the centre of the earth, and $\vec{r}_{\mathrm{spin}}$ is the vector from there to the detector. Correspondingly we have

$$\Delta\Phi(t) = 2\pi \Delta f \, t + \Delta\Phi_{\mathrm{orb}}(t) + \Delta\Phi_{\mathrm{spin}}(t) \,, \tag{14}$$

where

$$\Delta\Phi_{\mathrm{orb}} = \frac{2\pi}{c} \, \vec{r}_{\mathrm{orb}}(t) \cdot \vec{A} \,, \quad \text{and} \quad \Delta\Phi_{\mathrm{spin}} = \frac{2\pi}{c} \, \vec{r}_{\mathrm{spin}}(t) \cdot \vec{A} \,. \tag{15}$$

4.1. Spin motion of the earth

Except for very short observation times $T \ll 1$ day, which are not relevant for searches for continuous waves, the phase modulation Φ_{spin} due to the spin-motion of the earth is oscillatory, and can therefore not be treated using a Taylor-expansion. However, following an approach first used in [6, 10], it is more advantageous to use the Jacobi-Anger expansion, which allows one to expand an oscillatory exponent in terms of the Bessel-functions $J_n(z)$, namely

$$e^{iz\cos\zeta} = \sum_{n=-\infty}^{\infty} i^n \, J_n(z) \, e^{in\zeta} \,. \tag{16}$$

In order to be able to use this, we write the detector motion $\vec{r}_{\mathrm{spin}}(t)$ as

$$\vec{r}_{\mathrm{spin}}(t) = \sin\lambda \, R_\oplus \, \hat{z} + \cos\lambda \, R_\oplus \, \hat{\varpi}(t) \,, \tag{17}$$

where λ is the latitude of the detector, $R_\oplus$ is the radius of the earth, $\hat{z}$ is the unit-vector along the rotation axis and $\hat{\varpi}(t)$ is the time-dependent unit-vector orthogonal to $\hat{z}$, pointing from the rotation axis to the detector. Using this decomposition, we can write the phase-mismatch due to the spin-motion of the earth as

$$\Delta\Phi_{\mathrm{spin}}(t) = \Delta\Phi_z + K_A \, \cos\varphi(t) \,, \tag{18}$$

where we defined

$$\Delta\Phi_z \equiv 2\pi \frac{R_\oplus}{c} \sin\lambda \, A_z \,, \quad K_A \equiv 2\pi \frac{R_\oplus}{c} \cos\lambda \, A_\perp \,, \tag{19}$$

and

$$\varphi(t) = \varphi_A + \Omega_{\mathrm{spin}} \, t \,, \quad \text{with} \quad \varphi_A = \measuredangle \left(\vec{A}_\perp, \hat{\varpi}(0) \right) , \tag{20}$$

and where A_z and $\vec{A}_\perp$ are the parallel and orthogonal projections of $\vec{A}$ with respect to the rotation axis $\hat{z}$. Using this decomposition, we can apply the Jacobi-Anger expansion (16) as follows:

$$e^{i\Delta\Phi_{\rm spin}(t)} = e^{i\Delta\Phi_z} \sum_{n=-\infty}^{\infty} i^n \, e^{in\varphi_A} \, J_n(K_A) \, e^{i\,n\,\Omega_{\rm spin}\,t} \,. \tag{21}$$

Substituting this together with (14) into the matched-filtering amplitude (11), we obtain

$$X = e^{i\Delta\Phi_z} \sum_{n=-\infty}^{\infty} i^n \, e^{in\varphi_A} \, J_n(K_A) \, Y_n \,, \tag{22}$$

where

$$Y_n = \frac{1}{T} \int \exp\left[i \left(2\pi\Delta f \, t + \Delta\Phi_{\rm orb}(t) + n\,\Omega_{\rm spin}\,t\right)\right] \, dt \,. \tag{23}$$

4.2. Orbital motion around the sun

Contrary to the spin-motion, the orbital motion induces a slowly varying and non-oscillatory phase-correction for observation-times $T \ll 1$ year, so we can expand the orbital phase-mismatch $\Delta\Phi_{\rm orb}(t)$ in terms of the small quantity $\varepsilon \equiv \Omega_{\rm orb} T \ll 1$, which leads to

$$Y_n = e^{i\Delta\Phi_{\rm orb}(0)} \frac{1}{T} \int \exp\left[i \left(a_1\, t + \sum_{k=2} a_k t^k\right)\right] \, dt \,, \tag{24}$$

with the coefficients

$$\begin{aligned} \frac{a_1}{2\pi} &= \Delta f + \vec{\beta}_0 \cdot \vec{A} + n\, f_{\rm spin} \,, \\ \frac{a_k}{2\pi} &= \frac{1}{k!} \, \vec{\beta}_0^{\,(k-1)} \cdot \vec{A} \,, \qquad (k>1) \,, \end{aligned} \tag{25}$$

where we defined $f_{\rm spin} \equiv \Omega_{\rm spin}/2\pi$, and where $\vec{\beta}_0 \equiv \vec{V}_0/c = \dot{\vec{r}}_{\rm orb}(0)/c$ denotes the orbital velocity at the start of the observation $t = 0$.

Note that the integrals Y_n will be strongly peaked as a function of the index n, namely by considering

$$|Y_n| \approx \left| \frac{1}{T} \int e^{i a_1 t} \, dt \right| \sim \mathrm{sinc}\left[a_1 \frac{T}{2}\right] \,, \tag{26}$$

we see that Y_n will have a maximum for the index n^* closest to the point $a_1 = 0$, i.e.,

$$n^* = -\mathrm{round}\left[\frac{\Delta f + \vec{\beta}_0 \cdot \vec{A}}{f_{\rm spin}}\right] \,. \tag{27}$$

As a first approximation we therefore only keep the dominant term n^* in the Jacobi-Anger expansion, i.e., we set $Y_n \approx Y_{n*}\, \delta_{n,n*}$, and so we obtain for the matched-filtering amplitude

$$X \approx e^{i\Delta\Phi_z} \, i^{n*} \, J_{n*}(K_A) \, Y_{n*} \,. \tag{28}$$

We are interested in the regions of parameter-space where $|X| \sim \mathcal{O}(1)$. In these regions we can assume the exponent in (24) to be small, and therefore, after Taylor-expanding and integrating (24), we can obtain the approximate expression

$$|X|^2 \approx J_{n*}^2(K_A) \left[1 - \frac{\hat{a}_1^2}{12}\, T^2 - \frac{\hat{a}_1 a_2}{6}\, T^3 + \mathcal{O}(T^4)\right] \equiv |X_1|^2 \,, \tag{29}$$

where $\hat{a}_1 \equiv a_1(n^*)$.

5. The 'maximum structure' of $|X|$

On can see from its definition (11) that $|X|$ has a global maximum of $|X| = 1$ in the perfectly matched case ($f = f_\mathrm{s}$ and $\vec{n} = \vec{n}_\mathrm{s}$), while it will be nearly zero almost everywhere else, because generally $\Delta\Phi$ will not be small. Guided by the observed structure of the detection statistic (see section 6, for example), we focus on the points in parameter space where $|X|$ (or $\mathcal{F}$) has a local maximum in target-frequency f for a fixed sky-position $\vec{n}$, i.e.,

$$\left.\frac{\partial |X|^2}{\partial f}\right|_{\vec{n}} = 0\,. \tag{30}$$

In order to understand the qualitative features of these local maxima, we now also neglect the spin motion of the earth (setting $n^* = 0$ and $K_A = 0$), and using (29) and (25) we obtain the following condition for local maxima (in the sense of (30)):

$$a_1 a_1' + a_2\, T a_1' + a_1\, T a_2' = 0\,, \tag{31}$$

where we write $a_k' \equiv \partial_f a_k(f, \vec{n})$. We can solve this order by order in T (strictly speaking, in the small parameter $\varepsilon = \Omega_\mathrm{orb} T$), and to zeroth order we find

$$\mathcal{O}(T^0): \quad a_1\, a_1' = 0 \quad \Longrightarrow \quad \Delta f + \vec{\beta}_0 \cdot \vec{A} = 0\,, \tag{32}$$

as $a_1' = \mathcal{O}(1)$. For the next order we therefore solve (31) with the ansatz $a_1 = \lambda T$ (with $\lambda = \mathcal{O}(1)$), so we find

$$\mathcal{O}(T): \quad a_1 + a_2 T = 0 \quad \Longrightarrow \quad \Delta f + \vec{\beta}_1 \cdot \vec{A} = 0\,, \tag{33}$$

where $\vec{\beta}_1 \equiv \vec{\beta}_0 + \dot{\vec{\beta}}_0 \,\frac{T}{2}$ is the first order approximation of the orbital velocity at the midpoint of the observation time. This scheme can be extended to arbitrary order in T, but for the qualitative discussion here we restrict ourselves to first order. The condition (33) can be expressed more explicitly as

$$f\left(1 + \vec{\beta}_1 \cdot \vec{n}\right) = f_\mathrm{s}\left(1 + \vec{\beta}_1 \cdot \vec{n}_\mathrm{s}\right)\,. \tag{34}$$

For a given signal $\{\vec{n}_\mathrm{s}\,, f_\mathrm{s}\}$, this equation describes the (approximate) location of the local maxima of $|X|$ as a function of f for fixed $\vec{n}$. Conversely this can be regarded at fixed frequency f, describing the sky-locations $\vec{n}$ in which the maximum occurs at this particular frequency f. From the above equation one can easily see that these points $\vec{n}$ describe a circle in the sky, which has its centre in $\vec{\beta}_1$, and an opening angle determined by the signal-location and the target frequency. In the case $f = f_\mathrm{s}$, we see that $\vec{n} = \vec{n}_\mathrm{s}$ is one of the possible solutions of (34), and so the circle will pass through the signal-location in the sky. If $f < f_\mathrm{s}$, then we must have $\vec{\beta}_1 \cdot \vec{n} > \vec{\beta}_1 \cdot \vec{n}_\mathrm{s}$, i.e., the opening angle of the circle has to be larger than in the case of a perfectly matched target-frequency, and vice-versa for the case of $f > f_\mathrm{s}$. For a 10-hour integration starting at GPS-time $t_0 = 732490940$ s, the orbital velocity at the midpoint is $\vec{\beta}_1 = [0.36, -9.13, -3.96] \times 10^{-5}$, and the corresponding family of circles is shown in figure 1. This equation also determines the upper limit on the frequency-mismatch Δf for which such a local maximum is possible, namely, by rewriting (34) as

$$\left|\frac{\Delta f}{f_\mathrm{s}}\right| = \frac{\left|\vec{\beta}_1 \cdot \Delta\vec{n}\right|}{\left|1 + \vec{\beta}_1 \cdot \vec{n}\right|} \leq \frac{2\beta_1}{1 - \beta_1} = 2\beta_1 + \mathcal{O}(\beta_1^2)\,, \tag{35}$$

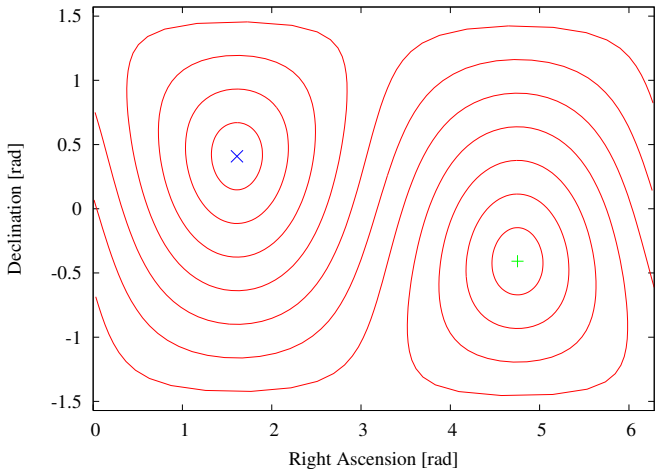

Figure 1. Family of circles described by (34) for a $T = 10$ hours observation starting at GPS-time $t_0 = 732490940$ s. The direction of $\vec{\beta}_1$ is marked by '×', while '+' indicates the direction $-\vec{\beta}_1$.

we see that the maximal relative frequency-mismatch is bounded by *twice* the Doppler-shift due to the orbital velocity. Using the value $V_{\mathrm{orb}} \approx 3\times 10^4$ m s^{-1}, this corresponds to a "Doppler-window" of $\Delta f/f \sim \pm 2 \times 10^{-4}$.

We note another interesting property of the approximate expression (29) for the matched-filtering amplitude $|X|$: namely, from the above discussion we know that the local maxima of $|X|$ occur on or close to the circles described by (34), which are characterised by $a_1 \approx 0$. Therefore we see from (29) that the amplitude of $|X_1|$ along these circles will be dominated by the factor $J_{n*}(K_A)$, where K_A is proportional to $A_\perp$, the projection of $\vec{A}$ into the equatorial plane. This factor is therefore symmetrical in the target sky-position $\vec{n}$ with respect to the equatorial plane, a feature which can indeed be seen in the plot of (29) shown in figure 4(b). Interestingly, this symmetry *can* still be present in the fully numerical $\mathcal{F}$-statistic, as seen, for example, in figure 3(b), while the effects of spin-motion and antenna-patterns can also mask this feature depending on the parameters, as seen in figure 3(a).

6. Comparison to fully numerical results for the $\mathcal{F}$-statistic

We now turn to comparing these analytic results to the actual parameter-space structure of the fully numerical $\mathcal{F}$-statistic including all effects of amplitude-modulation and using an ephemeris-based description of the detector-motion. As an example, we consider a 10-hour observation time starting at GPS-time $t_0 = 732490940$ s, and we use a fake pulsar-signal at $f_{\mathrm{s}} = 100$ Hz and sky-position $(\alpha_{\mathrm{s}}, \delta_{\mathrm{s}}) = (2, 1)$, for two different choices of amplitude-parameters shown in table 1. In the following the detector-location is always chosen to be the LIGO Livingston Observatory (LLO), and we only consider pure signals without noise. The fake pulsar-signal is generated using `makefakedata_v4`, and the $\mathcal{F}$-statistic [5] is calculated using `ComputeFStatistic`‡.

‡ These codes are found in `LALApps`[1], under `src/pulsar/Injections` and `src/pulsar/FDS_isolated`.

Table 1. Amplitude- and phase-parameters of two fake pulsar-signals.

Model	f [Hz]	(α, δ) [rad]	A_+	$A_\times$	Ψ	Φ_0
I	100	(2.0, 1.0)	1.0	0.5	1.0	2.0
II	100	(2.0, 1.0)	1.0	0.0	0.0	0.0

We observe the following structure of the $\mathcal{F}$-statistic over the parameter space $\{\alpha, \delta, f\}$: searching over the sky at a perfectly matched target-frequency $f = f_\mathrm{s}$, the $\mathcal{F}$-statistic has a maximum at the signal sky-position $(\alpha_\mathrm{s}, \delta_\mathrm{s})$, as expected, but remains of the same order on a very narrow, complete circle over the sky (obviously including the signal-position), while it is practically zero everywhere else. For mismatched target-frequencies f (within the Doppler-window of f_s), there is a different but concentric circle of $\mathcal{F}$-values comparable to the maximum, with a larger radius for $f < f_\mathrm{s}$, and a smaller radius for $f > f_\mathrm{s}$, as shown in figure 2. This agrees qualitatively and quantitatively surprisingly well with the circle-structure predicted solely based on the effect of the orbital Doppler-shift, i.e., (34) and figure 1.

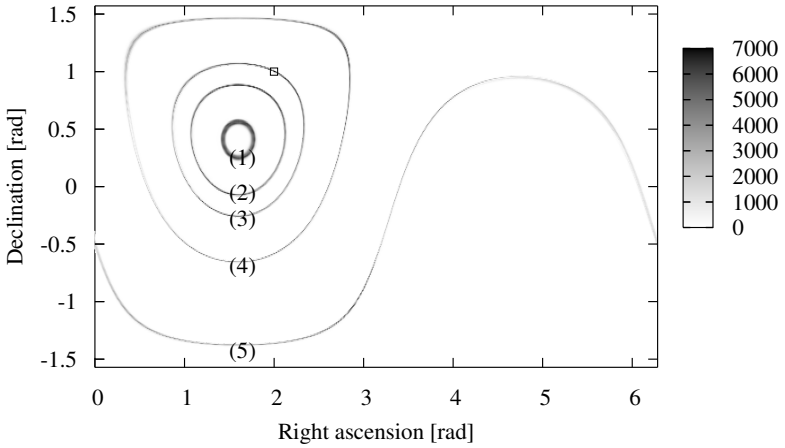

Figure 2. Plot of the $\mathcal{F}$-statistic over the sky superposed for different target frequencies f: (1) $f = 100.002$ Hz, (2) $f = 100.001$ Hz, (3) $f = f_\mathrm{s} = 100$ Hz, (4) $f = 99.997$ Hz and (5) $f = 99.99$ Hz. The parameters of the injected signal correspond to model I in table 1, and the small square indicates the sky-position of the signal.

In the next step we run an all-sky search over the whole Doppler-window $f \in (1 \pm 2 \times 10^{-4})\, f_\mathrm{s}$, corresponding to a dense superposition of these circles for the different target-frequencies. The resulting $\mathcal{F}$-statistic projected on the sky is shown in figure 3(a) and (b) for pulsar-signals I and II, respectively. From these projected plots we see more clearly that the variation of the amplitude of the $\mathcal{F}$-statistic maxima is more sensitive to the polarisation-parameters of the signal, due to effects of the antenna-pattern. For example, figure 3(b) shows some of the equatorial symmetry characteristic for the approximate expression (29), as discussed in section 5, in particular we see a mirror-image in $(2, -1)$ of the absolute maximum at the signal-position $(2, 1)$. For signal I, on the other hand, the projected $\mathcal{F}$ is more asymmetrical

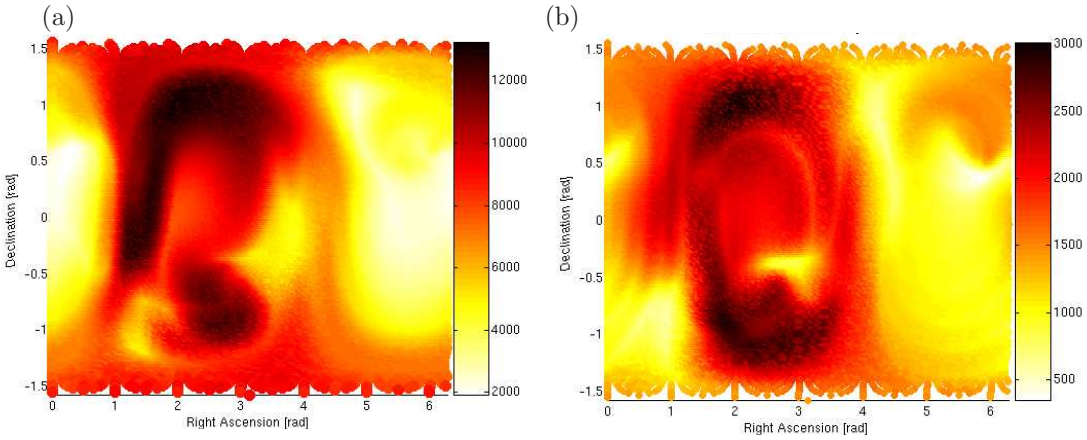

Figure 3. Projected $\mathcal{F}$-statistic over the sky in the frequency range $f \in (1 \pm 2 \times 10^{-4})\, f_{\mathrm{s}}$ for (a) pulsar-signal I and (b) signal II as defined in table 1.

and there is no mirror-image of the maximum in the southern hemisphere.

Summarising these observations we can state that the *locations* of the local maxima of $\mathcal{F}$ are dominantly determined by the orbital velocity of the earth, and are described very well§ by the circles (34), independently of detector-location and amplitude-parameters of the signal. The spin-motion of the detector and amplitude-modulation due to the rotating antenna-pattern, on the other hand, are responsible for the variation of the amplitude of $\mathcal{F}$ along these circles, as seen in figure 3.

Finally, we plot the approximate detection amplitude $|X_1|^2$ given by (29) over the sky for different target frequencies, as shown in figure 4(a), which shows some striking similarities to the 'exact' result in figure 2. In particular, it exhibits the feature of vanishing very rapidly outside the narrow "circles" described approximately by (34). The amplitude of $|X_1|^2$ on the circles, however, is not a good description of the corresponding $\mathcal{F}$-statistic amplitude, as $|X_1|^2$ is seen to be much more strongly peaked around the signal-location and decreases rather rapidly to about 0.1 on most of the circles (see figure 4(b)), while the $\mathcal{F}$-statistic has a similar amplitude to the maximum over most of the circles. Note also that figure 4(b) illustrates the equatorial symmetry of $|X_1|^2$ as discussed at the end of section 5.

7. Discussion

In a practical search for continuous gravitational waves we will usually be interested in the highest values ("candidates") of $\mathcal{F}$ over a chosen volume of the parameter-space. From the results presented here we expect that a real signal would generate candidates nearly everywhere on the sky within the Doppler-window $\pm 2 \times 10^{-4}$ of the signal-frequency f_{s}. All these candidates, however, will satisfy (34) with an (approximately) identical value on the right-hand side, and so the quantity $\kappa \equiv f(1 + \vec{\beta}_1 \cdot \vec{n})$ is an (approximate) invariant of candidates caused by the same signal. This could be a very useful criterion for classifying equivalent candidates, and also for determining

§ A preliminary numerical comparison of the frequency $f_{\mathcal{F}}$ of the maximum of $\mathcal{F}$ for a fixed sky-position $\vec{n}$ and the theoretical prediction f_{th} from (34) yields the bound $|f_{\mathcal{F}} - f_{\mathrm{th}}|/f_{\mathcal{F}} < 10^{-6}$ over the whole sky.

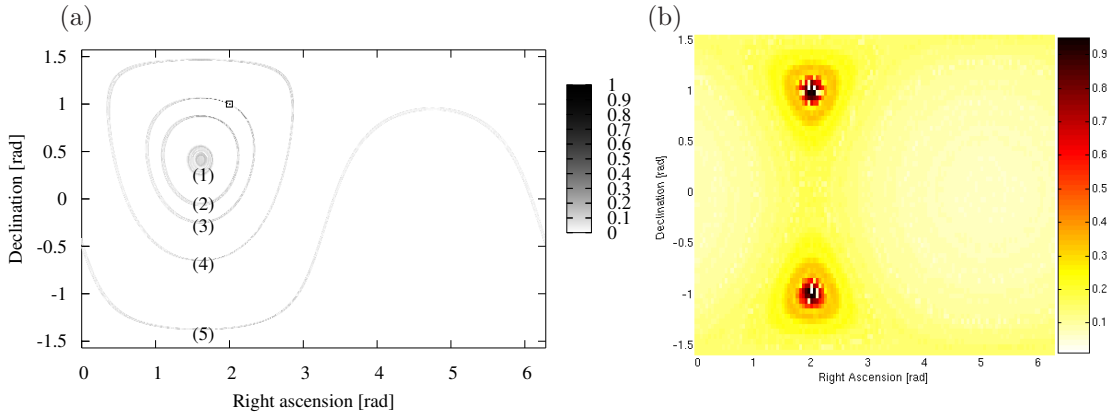

Figure 4. Plot of the approximate matched-filtering amplitude $|X_1|^2$ over the sky for (a) different target frequencies (1) $f = 100.002$ Hz, (2) $f = 100.001$ Hz, (3) $f = f_s = 100$ Hz, (4) $f = 99.997$ Hz and (5) $f = 99.99$ Hz, and (b) over the whole Doppler-window $f \in (1 \pm 2 \times 10^{-4})\, f_s$ projected on the sky. The small square indicates the sky-position of the signal (model I in table 1).

coincident candidates from different detectors. One could further use this to construct coincidence-tests of candidates from different observation times, as $\vec{\beta}_1(t)$ is a known function of time. In order for these methods to be practically useful, however, the errors of the different approximations need to be quantified, and we need to test the robustness of the suggested coincidence criteria in the presence of noise.

Acknowledgments

We would like to thank Badri Krishnan, Maria Alessandra Papa, Xavier Siemens and Alicia Sintes for helpful discussions.

References

[1] LALApps, a collection of software tools for data-analysis (using `LAL`). `http://www.lsc-group.phys.uwm.edu/daswg/projects/lalapps.html`.
[2] Abbot B *et al* (LIGO Scientific Collaboration) 2004 *Phys. Rev.* D **69** 082004
[3] Abbot B *et al* (LIGO Scientific Collaboration) 2005 *to appear in PRL Preprint* gr-qc/0410007
[4] Brady P R, Creighton T, Cutler C, Schutz B F 1998 *Phys. Rev.* D **57** 2101–2116
[5] Jaranowski P, Królak A, Schutz B F 1998 *Phys. Rev.* D **58** 063001
[6] Jotania K, Valluri S R, Dhurandhar S V 1996 *Astron. Astrophys.* **306** 317–325
[7] Krishnan B, Sintes A M, Papa M, Schutz B F, Frasca S, Palomba C 2004 *Phys. Rev.* D **70** 802001
[8] Owen B J 1996 *Phys. Rev.* D **53** 6749–6761
[9] Astone P *et al* 2003 *Class. Quantum Grav.* **20** 665
[10] Valluri S R, Drozd J J, Chishtie F A, Biggs R G, Davison M, Dhurandhar S V, Sathyaprakash B S 2002 *Class. Quantum Grav.* **19** 1327–1334